

ON NUMERICALLY ACCURATE FINITE ELEMENT SOLUTIONS IN THE FULLY PLASTIC RANGE

J.C. NAGTEGAAL *, D.M. PARKS and J.R. RICE

Division of Engineering, Brown University, Providence, R.I., U.S.A.

Received 17 April 1974

Revised manuscript received 8 May 1974

It is often found that tangent-stiffness finite element solutions for elastic-plastic materials exhibit much too stiff a response in the fully plastic range. This is most striking for the perfectly plastic material idealization, in which case a limit load exists within conventional small displacement gradient assumptions. However, finite element solutions often exceed the limit load by substantial amounts, and in some cases have no limit load at all. It is shown that a cause of this inaccuracy is that incremental deformation fields of typical two and three-dimensional finite elements are highly constrained at or near the limit load. This is shown to enforce unreasonable kinematic constraints on the modes of deformation which assemblages of elements are capable of exhibiting. A general criterion for testing a mesh with topologically similar repeat units is given, and the analysis shows that only a few conventional element types and arrangements are, or can be made, suitable for computations in the fully plastic range. Further, a new variational principle, which can easily and simply be incorporated into an existing finite element program, is presented. This allows accurate computations to be made even for element designs that would not normally be suitable. Numerical results are given for three plane strain problems, namely pure bending of a beam, a thick-walled tube under pressure, and a deep double edge cracked tensile specimen. These illustrate the effects of various element designs and of the new variational procedure. An appendix extends the discussion to elastic-plastic computation at finite strain.

1. Introduction

In recent years, the finite element method has been employed for analysis of structures exhibiting elastic-plastic material behavior [1], and many successful applications have been made (see [2] for a comparison of possible forms of the required incremental analysis). However, with the application of the method, at least in its tangent-stiffness form, to problems of plane strain, axisymmetric, and three-dimensional problems, inaccurate results are often obtained. The problem is most clearly demonstrated for structures of ideally plastic material. Then a limit load exists which can sometimes be calculated exactly or bounded from above by the kinematical theorem, while the finite element solution often seems to exhibit no limit load at all, but rather a steadily rising load-displacement curve attaining values far in excess of the true limit load. Similarly, for strain-hardening materials having typical values for the plastic tangent modulus of two or more orders of magnitude less than the elastic modulus, the finite element solution exhibits an artificially high terminal slope of the load-deflection curve in the fully plastic range.

Later we shall see examples of this for a beam in pure bending and for a punch problem. In the case of a plane strain extrusion problem [3], when a bilinear constitutive law with slight plastic

* Currently 570 Ordnance Regiment, Royal Dutch Army.

work-hardening ($d\bar{\sigma}/d\bar{\epsilon}_p \equiv H = 4.4 \times 10^{-3} E$, where E is the Young's modulus) was incorporated, a finite element extrusion pressure of 1.5 times a slip-line solution (using the same yield stress as the linearly hardening model) was attained with overall billet displacements only of order six times the displacement obtained at the slip line limit load. This indicates that the computed stiffness in the fully plastic range far exceeds what would be expected for the small hardening modulus used.

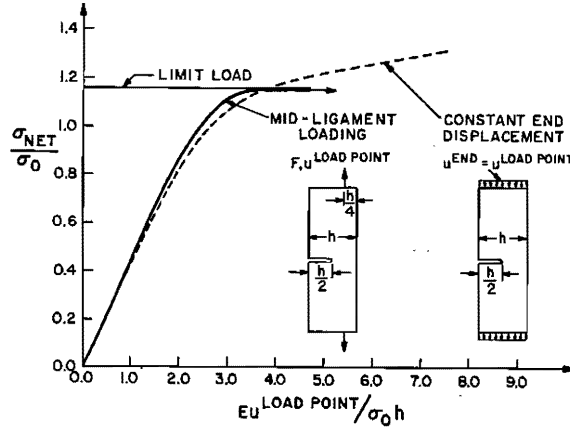


Fig. 1. Load-displacement curves obtained from finite element solutions of plane strain single edge cracked tensile specimens subjected to mid-ligament loading and constant end displacement boundary conditions.

In some cases, however, the correct limit load is obtained. Fig. 1 illustrates some of the peculiarities which have been encountered by the authors and co-workers in elastic-perfectly plastic analysis of plane strain bodies containing cracks. The finite element meshes shown in fig. 2 were used to solve the single-edge notched plane strain tensile specimen subject to both uniform end displacement [4] (i.e., no end rotation) and the static equivalent of a mid-ligament concentrated force. These two loading conditions have the same analytical limit load, namely, twice the yield stress in shear on the net section. As can be seen in fig. 1, the overall load-deflection curves of the two loading conditions are quite different in the fully plastic regime. The solution for the mid-ligament loading clearly indicates the correct limit load, while the constant end displacement solution exceeds the limit load, with the load continuing to rise at a roughly constant rate.

A cause of these problems relates to the fact that the deformation state of an elastic-perfectly plastic material is highly constrained at limit load; for the usual material idealization, deformation increments at limit load will be *strictly incompressible*. In the usual finite element formulation, in terms of kinematically admissible displacement fields, the same condition will have to be satisfied.

In particular, a tangent-stiffness finite element solution satisfies the incremental virtual work principle

$$\int_S \dot{T}_i \dot{u}_i dS = \sum_{elem.} \int_{V_{elem.}} \dot{\sigma}_{ij} \dot{\epsilon}_{ij} dV_{elem.}, \quad (1.1)$$

precisely, where $\dot{\sigma}_{ij}$ is the stress rate following from the prescribed constitutive law in terms of the current stress σ_{ij} and strain rate $\dot{\epsilon}_{ij}$ within each element. This stress rate can be written as

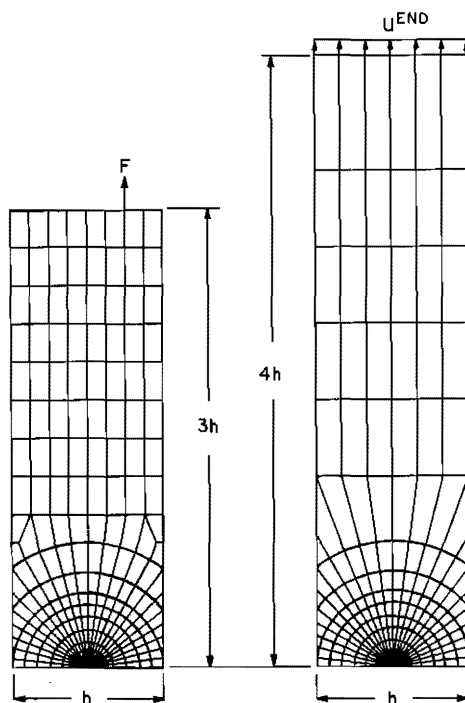


Fig. 2. Finite element meshes used to solve the mid-ligament loading and constant end displacement single edge cracked tensile specimens.

$$\dot{\sigma}_{ij} = \dot{s}_{ij} + \frac{1}{3} \delta_{ij} \dot{\sigma}_{kk} , \quad (1.2)$$

where \dot{s}_{ij} is the deviatoric stress increment. Since the plastic deformation will be assumed purely deviatoric, the hydrostatic stress increment $\frac{1}{3} \dot{\sigma}_{kk}$ can be expressed as

$$\frac{1}{3} \dot{\sigma}_{kk} = \kappa \dot{\epsilon}_{kk} , \quad (1.3)$$

where

$$\kappa = E/3(1 - 2\nu) \quad (1.4)$$

is the elastic bulk modulus and $\dot{\epsilon}_{kk}$ is the dilatational strain increment. Substitution of (1.2) and (1.3) in (1.1) then furnishes

$$\int_S \dot{T}_i \dot{u}_i dS = \sum_{elem.} \int_{V_{elem.}} [\dot{s}_{ij} \dot{e}_{ij} + \kappa (\dot{\epsilon}_{kk})^2] dV_{elem.} , \quad (1.5)$$

where \dot{e}_{ij} is the deviatoric strain increment. In the vicinity of the limit load, the term $\dot{s}_{ij} \dot{e}_{ij}$ will tend to vanish pointwise, but, as follows from plastic normality, will never be negative. Hence, from (1.5), this implies that the incremental finite element solution satisfies

$$\int_S \dot{T}_i \dot{u}_i dS \geq \sum_{elem.} \int_{V_{elem.}} \kappa (\dot{\epsilon}_{kk})^2 dV_{elem.} \quad (1.6)$$

The following result may thus be stated:

In order for a limit load to exist for the discretized finite element model of an elastic-plastic problem, it is necessary that the elements be capable of deforming so that $\dot{\epsilon}_{kk} = 0$ pointwise throughout the elements. Otherwise (1.6) requires that the load-deflection curve be steadily rising — i.e. no limit load exists.

In the next section it will be shown that, except for plane stress problems, the requirement $\dot{\epsilon}_{kk} = 0$ severely constrains the class of deformations of which typical finite element grids are capable. When they are forced to deform in such a constrained fashion, unreasonably high limit loads, or no limit loads at all, will result. On the other hand, even if no limit load is achieved in the finite element formulation, it is to be expected (and is indeed observed) that the slope of the load-deflection curve is reduced substantially from its initial elastic value at load levels near the theoretical limit load. This, however, does not allow an accurate inference of the limit load.

Even if the material is linearly work-hardening with a small hardening coefficient, the terminal slope of the load-deflection curve will not necessarily be accurately determined (as was argued previously and will be demonstrated in an example), since the material will deform in a nearly incompressible fashion in the fully plastic range.

It is clear that the problems discussed here have a strong similarity to problems encountered in the analysis of incompressible fluids and rubber-like solids. The difference is that the material behaves incompressibly only as limit conditions are approached because the effective shear modulus then tends to vanish, whereas fluids and rubber-like solids behave incompressibly from the start because the bulk modulus is very large. The essential problem is the same in both cases, however, in the sense that the incompressibility requirement puts too severe constraints on the possible deformation modes.

2. Analysis

In the previous section, it has been observed that elements must be capable of deforming without change of volume pointwise if a limit load is to be obtained. It is therefore useful to investigate the constraints this enforces upon each element, and the effect of these constraints on the behavior of an assemblage of elements.

Consider, for instance, the grid of 4-node rectangular isoparametric elements shown in fig. 3. Within each element, the displacement increments are of the form

$$\dot{\mathbf{u}} = \begin{Bmatrix} \dot{u}_x \\ \dot{u}_y \end{Bmatrix} = \mathbf{a} + \mathbf{b}x + \mathbf{c}y + \mathbf{d}xy, \quad (2.1)$$

where the vectors \mathbf{a} , \mathbf{b} , etc. are expressed in terms of the nodal velocities and coordinates. Now, the incompressibility constraint for plane strain has the form

$$\dot{\epsilon}_{xx} + \dot{\epsilon}_{yy} = \frac{\partial \dot{u}_x}{\partial x} + \frac{\partial \dot{u}_y}{\partial y} = 0, \quad (2.2)$$

and this requires that $\mathbf{d} = \mathbf{0}$ as well as that $b_x + c_y = 0$, a total of *three* constraints.

The fact that $\mathbf{d} = \mathbf{0}$ means that at limit load each element has strain increments which are constant throughout the element. It is then evident from displacement continuity that all elements marked * in fig. 3 must have the same value of $\dot{\epsilon}_{xx}$, whereas all elements marked † must have the same value of $\dot{\epsilon}_{yy}$. Moreover, since $\dot{\epsilon}_{xx} = -\dot{\epsilon}_{yy}$, $\dot{\epsilon}_{xx}$ and $\dot{\epsilon}_{yy}$ will be the same in all elements marked * or †. Since a similar argument can be set up for any row and column, $\dot{\epsilon}_{xx}$ and $\dot{\epsilon}_{yy}$ must be the same in every element of the grid. Clearly, this is a very unrealistic constraint.

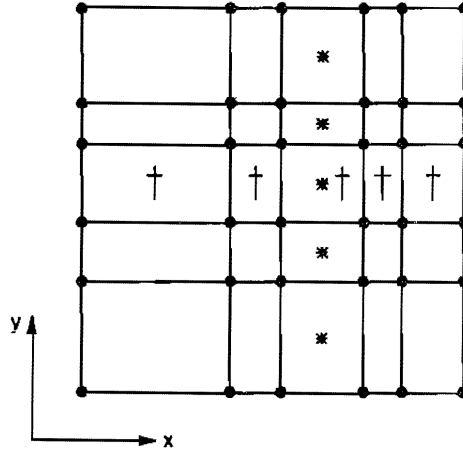


Fig. 3. Propagation of incompressibility constraints in a mesh of rectangular four-node isoparametric plane strain finite elements.

It is at least possible for this mesh to have a non-uniform shear $\dot{\epsilon}_{xy}$, but the situation is even worse in case the grid consists of arbitrary quadrilateral isoparametric elements. Within an element the displacement increments are of the form

$$\dot{\mathbf{u}} = \mathbf{a} + b\eta + c\xi + d\eta\xi, \quad (2.3)$$

where η and ξ are defined by

$$\begin{Bmatrix} x \\ y \end{Bmatrix} = \boldsymbol{\alpha} + \boldsymbol{\beta}\eta + \boldsymbol{\gamma}\xi + \boldsymbol{\delta}\eta\xi. \quad (2.4)$$

(See, for instance, [6].) A lengthy but straightforward calculation furnishes the *three* incompressibility constraints per element:

$$\begin{aligned} b_x \gamma_y - c_x \beta_y - b_y \gamma_x + c_y \beta_x &= 0, \\ b_x \delta_y - d_x \beta_y - b_y \delta_x + d_y \beta_x &= 0, \\ d_x \gamma_y - c_x \delta_y - d_y \gamma_x + c_y \delta_x &= 0. \end{aligned} \quad (2.5)$$

A solution to this system of equations in terms of three parameters A , B , and C is

$$\begin{aligned} b_x &= A\beta_x + B\beta_y, & b_y &= C\beta_x - A\beta_y, \\ c_x &= A\gamma_x + B\gamma_y, & c_y &= C\gamma_x - A\gamma_y, \\ d_x &= A\delta_x + B\delta_y, & d_y &= C\delta_x - A\delta_y. \end{aligned} \quad (2.6)$$

Substitution of (2.6) in (2.3) then makes it possible to eliminate η and ξ from (2.3) and (2.4) — this furnishes the displacement increments

$$\dot{u}_x = D + Ax + By, \quad \dot{u}_y = E + Cx - Ay, \quad (2.7)$$

where the constants D and E do not depend on A , B and C . Hence, if the incompressibility constraint is to be satisfied, the strain increments will be constant throughout the element.

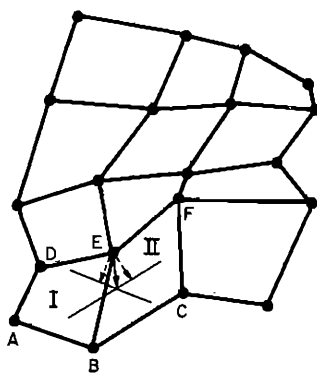


Fig. 4. Mesh of arbitrarily skewed four-node isoparametric plane strain finite elements.

This has catastrophic effects for an arbitrary grid. Consider, for instance, the grid in fig. 4, and specify the displacement increments of the three nodes A , B and C . Because the displacement increments of nodes A and B define the extensional strain along AB in element I, and because the element must deform with a constant strain of zero dilatation, we must then specify the component of displacement increment of node E in the direction normal to AB . Similarly, because the displacement increments of nodes B and C determine the extensional strain along BC in element II, we must also specify the displacement component of node E in the direction normal to BC . The incompressibility constraints of elements I and II then specify the components of displacement increment of node E in two linearly independent (though not orthogonal) directions. Thus the displacement increment vector of E is fully determined, and, in fact, it corresponds to that increment which causes identical strain increments in elements I and II. The displacement increments of nodes D and F are then also determined. Continuation of the argument then furnishes that the strain increment will be constant throughout the grid. It should be noted that this argument holds only if the element boundaries do not form a straight line through the body; over such a line the shear strain increment can be discontinuous.

Examples of the unreasonable constraints enforced by pointwise incompressibility upon displacement increment fields of other two and three-dimensional mesh configurations are given in Appendix 1.

We are now in a position to explain the results of fig. 1, bearing in mind a result of perfectly-plastic limit analysis: namely, that while the limit load is unique, the deformation field at limit load need not be unique. An acceptable limit field for both loading conditions, giving the correct limit load, is that of concentrated deformation on 45° lines from the crack tip to the surface, as shown in fig. 5a. An alternative limit field for the mid-ligament loading is shown in fig. 5b. This field consists of constant strain increments within the region bounded by the two 45° lines from the crack tip. The rest of the body is rigid, so the overall effect is that of a rotation of the two rigid regions about the crack tip. In fact, this was exactly the velocity field obtained at limit conditions in the finite element solution of the mid-ligament loading problem. Since the deforming regions do so uniformly, and the 45° lines coincide with element boundaries, the mesh of focused isoparametric quadrilaterals could readily accommodate the incompressibility constraints, hence leading to a very accurate finite element prediction of the limit load.

In contrast, however, the rotation produced by this field is incompatible with the constant end-displacement boundary condition of the other loading. The same constant strain pattern cannot develop, and an ever-worsening overestimate of the limit load results.

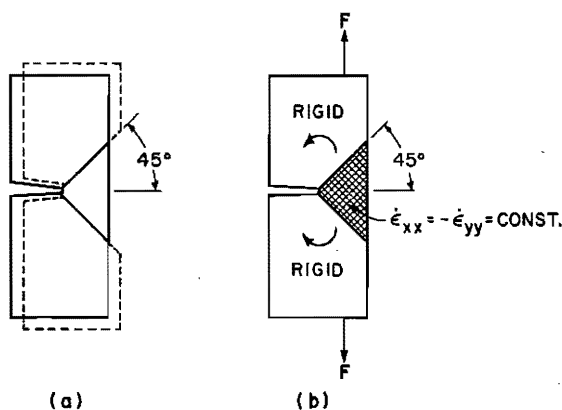


Fig. 5a. Acceptable limit mechanism for plane strain single edge notched tensile specimen subject to either mid-ligament loading or constant end displacement. b. Alternative limit mechanism for mid-ligament loading.

Although the problem has now been analyzed sufficiently for four-noded isoparametric quadrilateral elements, a more systematic approach is needed to find a solution to it. It is therefore useful to consider the matter of *convergence* of the solution if the mesh is refined. Refinement of the mesh will have two opposing effects:

- 1) It will increase the number of nodes, and since each node represents a specific number of degrees of freedom, it will increase the total number of degrees of freedom.
- 2) On the other hand, it will increase the number of elements, and since each element has a certain number of incompressibility constraints enforced upon itself, it will increase the total number of constraints.

It is clear that convergence will occur only if the total number of degrees of freedom increases

faster than the total number of constraints. This furnishes a relatively simple criterion to check whether a mesh of a certain type will be adequate to furnish accurate limit loads and flow fields. It should be noted that the total number of constraints is not always equal to the number of elements times the number of constraints per element. Sometimes elements can be arranged such that the constraints are no longer independent, an important example of which will be discussed in the next section. For the moment, however, these special cases will not be considered.

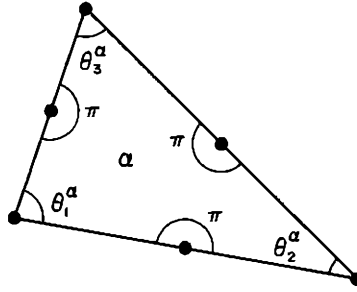


Fig. 6. Nodal angles for a linear strain triangular finite element.

It is thus important to determine the ratio of the total number of nodes to the total number of elements in the grid when it is refined. Consider a body, loaded in plane strain, the cross-section of which is subdivided into a mesh of elements of identical type. Define the nodal angles θ_i^α of an element α as the inner angle formed at the node by the two adjacent element boundaries. For each type of element the sum of these nodal angles is a given number. Consider, for instance, the six-noded triangle of fig. 6. Each of the nodal angles at the mid-points of the sides is equal to π radians, whereas the sum of the angles θ_1^α , θ_2^α and θ_3^α is also equal to π radians. Hence the sum of all nodal angles is equal to 4π radians. Similarly simple calculations can be made for other types of elements. For generality, let us assume that the sum of the nodal angles of a particular element type is equal to $n\pi$ radians. If the grid consists of p elements, then the sum of all nodal angles of all elements is equal to

$$\sum_{\alpha} \sum_i \theta_i^\alpha = pn\pi. \quad (2.8)$$

The sum of all nodal angles can also be calculated in a different way. Suppose the mesh has k nodes inside the body and l nodes on the boundary. The sum of the nodal angles around each interior node is equal to 2π radians, whereas the sum of the nodal angles at a boundary node is equal to $\pi - \gamma$ radians, where γ is a small angle due to the curvature of the boundary. In this way the sum is readily calculated as

$$\sum_{\alpha} \sum_i \theta_i^\alpha = (2k + l + 2c - 4)\pi, \quad (2.9)$$

where c is the degree of connectivity of the body ($c = 1$ if simply connected, etc.). From (2.8) and (2.9) then follows the equality

$$pn = 2k + l + 2c - 4, \quad (2.10)$$

or, alternatively,

$$\frac{p}{k} = \frac{2}{n} + \frac{l}{nk} + \frac{2c-4}{nk}. \quad (2.11)$$

Now if the mesh is refined, p , k , and l will all increase; hence the last term will vanish. Moreover, if the mesh is refined uniformly, k (the number of interior nodes) will increase approximately as the square of l (the number of boundary nodes). Hence

$$\lim_{k \rightarrow \infty} \left(\frac{p}{k} \right) = \frac{2}{n}. \quad (2.12)$$

Consider what this means for a grid of isoparametric quadrilateral elements. The sum of the nodal angles in one element is equal to 2π radians, and hence $n = 2$. Substitution in (2.12) then furnishes that in the limit the number of nodes will become equal to the number of elements. Since each node represents two degrees of freedom, and three incompressibility constraints are enforced upon each element, the total number of degrees of freedom is only $2/3$ of the total number of constraints. Hence convergence will not in general occur, which reaffirms the previously obtained result. Similar derivations can be made for other planar elements as well as for axisymmetric elements since (2.12) holds as well for this class. The results are displayed in table 1. The range of value of constraints per element from 6 to 8 given for the 8-noded quadrilateral depends on whether the sides of the element are linear or quadratic, respectively.

For three-dimensional elements, however, the ratio of nodes to elements is not unique, since the sum of the solid angles of a polyhedron is not a constant. Therefore one has to determine this ratio for a specific arrangement of elements. For some common regular grids, and thus of any grid which is equivalent, the results are displayed in table 2. It may be assumed that these results are fairly representative for most common types of arrangements.




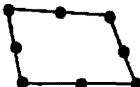




The results in tables 1 and 2 indicate that none of the usual finite elements, except the 6-noded plane strain triangle and, to a much lesser degree, the 10-noded tetrahedron, is adequate to analyze (approximately) incompressible, and thus limit load, behavior. Before going into a more systematic approach to solve the problem, let us consider what can be obtained by a special arrangement of the elements.

3. Special arrangements of elements

As has been mentioned previously, the total number of constraints is not necessarily equal to the product of the number of elements and the number of constraints per element. For special arrangements of elements, the total number of constraints may be less than this product. The obtained improvement, however, will be small, since it is necessary to combine a number of elements to eliminate one constraint. Thus this method will work only for elements for which the ratio of degrees of freedom to constraints in tables 1 and 2 is close or equal to one.

Table 1


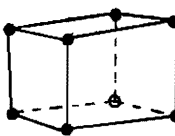
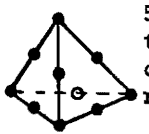
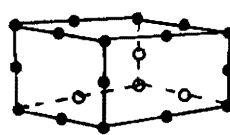
The effect of mesh refinement on the ratio of total degrees of freedom to total number of incompressibility constraints for some common two-dimensional finite elements.

	Element Type	$\frac{\text{Constraints}}{\text{Element}}$	$\frac{\text{Ratio Nodes}}{\text{Elements}}$	$\frac{\text{Ratio Deg. Freedom}}{\text{Constraints}}$
Plane Strain	 constant strain triangle	1	1/2	1
	 4-node quadrilateral	3	1	2/3
	 linear strain triangle	3	2	4/3
	 8-node quadrilateral	6 to 8	3	1 to 3/4
Axisymmetric		3	1/2	1/3
		5	1	2/5
		6	2	2/3
		≥ 9	3	$\leq 2/3$

Consideration of tables 1 and 2 with this in mind indicates that only a few types of elements could possibly be used for this purpose: for plane strain, the 3-noded triangular element and perhaps the 8-noded quadrilateral element, and for three-dimensional problems, the 10-noded tetrahedron. None of the axisymmetric elements could possibly be used. As yet the only successful arrangement that has been discovered is the combination of four 3-noded triangles as shown in fig. 7. Note that the triangular element boundaries form a quadrilateral "element" and its diagonals. This combination has the special property that if the incompressibility constraint is satisfied in three of the elements, the constraint in the fourth element is automatically satisfied. This brings the ratio of degrees of freedom to constraints from 1 to 4/3, which makes the arrangement suitable for analysis near limit load. The proof of this special property is given below.

Table 2

The effect of mesh refinement on the ratio of total degrees of freedom to total number of incompressibility constraints for some common arrangements of three-dimensional finite elements.

Element Type and Arrangement	Constraints Element	Ratio Nodes Elements	Ratio Deg.Freedom Constraints
 5 constant strain tetrahedra in cube; cubes in regular lattice	1	1/5	3/5
 8-node isoparametric cubes in regular lattice	7	1	3/7
 5 linear strain tetrahedra in cube; cubes in regular lattice	4	7/5	21/20
 20-node isoparametric cubes in regular lattice	≥ 16	4	$\leq 3/4$

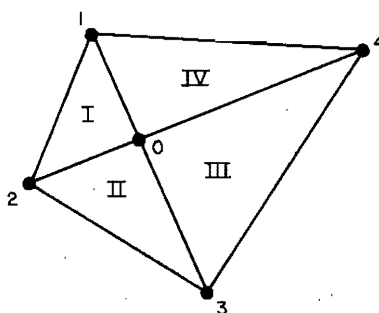


Fig. 7. Four constant strain triangular finite elements arranged to form a quadrilateral and its diagonals.

Let the coordinates of the node i be x_i , and let the node have a displacement increment \dot{u}_i . The area A of element I before the displacement increment has taken place is then equal to

$$A = \frac{1}{2} [(x_2 - x_0) \times (x_1 - x_0)] \cdot k, \quad (3.1)$$

where \times and \cdot denote the usual vector and scalar products respectively, and \mathbf{k} is the unit vector perpendicular to the plane of the elements. Similarly one finds that after the displacement increment has taken place,

$$A + \dot{A} = \frac{1}{2}[(\mathbf{x}_2 + \dot{\mathbf{x}}_2 - \mathbf{x}_0 - \dot{\mathbf{x}}_0) \times (\mathbf{x}_1 + \dot{\mathbf{x}}_1 - \mathbf{x}_0 - \dot{\mathbf{x}}_0)] \cdot \mathbf{k} . \quad (3.2)$$

Subtraction of (3.1) from (3.2) furnishes

$$\dot{A} = \frac{1}{2}[(\mathbf{x}_2 - \mathbf{x}_0) \times (\dot{\mathbf{x}}_1 - \dot{\mathbf{x}}_0) - (\mathbf{x}_1 - \mathbf{x}_0) \times (\dot{\mathbf{x}}_2 - \dot{\mathbf{x}}_0) + (\dot{\mathbf{x}}_2 - \dot{\mathbf{x}}_0) \times (\dot{\mathbf{x}}_1 - \dot{\mathbf{x}}_0)] \cdot \mathbf{k} . \quad (3.3)$$

When one neglects the second order terms, the incompressibility constraint takes the form

$$(\mathbf{x}_2 - \mathbf{x}_0) \times (\dot{\mathbf{x}}_1 - \dot{\mathbf{x}}_0) = (\mathbf{x}_1 - \mathbf{x}_0) \times (\dot{\mathbf{x}}_2 - \dot{\mathbf{x}}_0) . \quad (3.4)$$

Similarly, for the elements II and III, one obtains

$$(\mathbf{x}_3 - \mathbf{x}_0) \times (\dot{\mathbf{x}}_2 - \dot{\mathbf{x}}_0) = (\mathbf{x}_2 - \mathbf{x}_0) \times (\dot{\mathbf{x}}_3 - \dot{\mathbf{x}}_0) , \quad (3.5)$$

$$(\mathbf{x}_4 - \mathbf{x}_0) \times (\dot{\mathbf{x}}_3 - \dot{\mathbf{x}}_0) = (\mathbf{x}_3 - \mathbf{x}_0) \times (\dot{\mathbf{x}}_4 - \dot{\mathbf{x}}_0) . \quad (3.6)$$

Now multiply (3.4) by $|\mathbf{x}_3 - \mathbf{x}_0|/|\mathbf{x}_1 - \mathbf{x}_0|$, furnishing

$$\frac{|\mathbf{x}_3 - \mathbf{x}_0|}{|\mathbf{x}_1 - \mathbf{x}_0|} (\mathbf{x}_2 - \mathbf{x}_0) \times (\dot{\mathbf{x}}_1 - \dot{\mathbf{x}}_0) = -(\mathbf{x}_3 - \mathbf{x}_0) \times (\dot{\mathbf{x}}_2 - \dot{\mathbf{x}}_0) , \quad (3.7)$$

since $\mathbf{x}_3 - \mathbf{x}_0$ and $\mathbf{x}_1 - \mathbf{x}_0$ have opposite directions. Similarly, one obtains for (3.6)

$$-(\mathbf{x}_2 - \mathbf{x}_0) \times (\dot{\mathbf{x}}_3 - \dot{\mathbf{x}}_0) = \frac{|\mathbf{x}_2 - \mathbf{x}_0|}{|\mathbf{x}_4 - \mathbf{x}_0|} (\mathbf{x}_3 - \mathbf{x}_0) \times (\dot{\mathbf{x}}_4 - \dot{\mathbf{x}}_0) . \quad (3.8)$$

Substitution of (3.7) and (3.8) in (3.5) then furnishes

$$\frac{|\mathbf{x}_3 - \mathbf{x}_0|}{|\mathbf{x}_1 - \mathbf{x}_0|} (\mathbf{x}_2 - \mathbf{x}_0) \times (\dot{\mathbf{x}}_1 - \dot{\mathbf{x}}_0) = \frac{|\mathbf{x}_2 - \mathbf{x}_0|}{|\mathbf{x}_4 - \mathbf{x}_0|} (\mathbf{x}_3 - \mathbf{x}_0) \times (\dot{\mathbf{x}}_4 - \dot{\mathbf{x}}_0) , \quad (3.9)$$

or, alternatively,

$$\frac{|\mathbf{x}_4 - \mathbf{x}_0|}{|\mathbf{x}_2 - \mathbf{x}_0|} (\mathbf{x}_2 - \mathbf{x}_0) \times (\dot{\mathbf{x}}_1 - \dot{\mathbf{x}}_0) = \frac{|\mathbf{x}_1 - \mathbf{x}_0|}{|\mathbf{x}_3 - \mathbf{x}_0|} (\mathbf{x}_3 - \mathbf{x}_0) \times (\dot{\mathbf{x}}_4 - \dot{\mathbf{x}}_0) . \quad (3.10)$$

With the same argument as was used for (3.7) and (3.8) this yields

$$(\mathbf{x}_4 - \mathbf{x}_0) \times (\dot{\mathbf{x}}_1 - \dot{\mathbf{x}}_0) = (\mathbf{x}_1 - \mathbf{x}_0) \times (\dot{\mathbf{x}}_4 - \dot{\mathbf{x}}_0) ,$$

which proves that the incompressibility constraint in element IV is satisfied.

It should be noted that this approach requires no modification of existing finite element programs. The groups of four elements have all the generality in application of the usual quadrilateral elements, and the calculations can be carried out without changes to an already existing program. The principal shortcoming of the method is that it can be applied only to problems of plane strain, for which another alternative (the 6-noded triangular element) already exists. Even this alternative can be *slightly* improved by arranging the 6-noded elements similar to the 3-nodes ones. The ratio of degrees of freedom to constraints then improves from 4/3 to 16/11.

It should also be noted that the degrees of freedom available need not actually be incorporated into the finite element solution. For example the degrees of freedom corresponding to the interior node "0" of fig. 7 may be "condensed out" of the master stiffness matrix and recovered later. (See, for example, [7].)

As yet no method has been devised to arrange the 10-noded tetrahedra such that an acceptable ratio of degrees of freedom to constraints is obtained. Therefore a different, more general approach is needed to solve problems other than those of plane strain.

4. A modified variational principle

It has been discussed before that an absolute requirement for the existence of a limit load is that the dilatation increment $\dot{\epsilon}_{kk}$ vanishes pointwise. It has also been demonstrated that only a few of the conventional element types are, or can be made, useful to analyze problems under this constraint. Therefore it is desired that different elements be constructed for which fewer constraints per element are sufficient to satisfy the incompressibility requirement. This goal can be obtained by taking care that the dilatation is governed by fewer parameters than in the conventional elements. Clearly, this procedure may be applied only to higher order elements for which the conventional number of constraints per element exceeds unity. Theoretically it is possible to construct interpolation functions that have this property; in fact, if the arrangement in fig. 7 is taken as a single element, and the displacement of node 0 is chosen such that the dilatation in all subelements I through IV is the same, one has obtained such a function. This special field must, however, be considered as a "lucky guess", and a general approach to construct similarly simple fields for other elements does not seem to exist.

An alternative way to solve the problem is to create a variational principle in which the dilatational strain increment and the displacement increments are present as independent variables. We then have complete freedom to characterize the dilatation by as many (or as few) parameters as we choose. Such a variational principle is akin to the Hellinger–Reissner principle [8], which admits the displacements and the stresses as independent variables. The validity of the present principle will, however, be proved here independently of the H–R principle.

Consider the functional

$$I = I[\dot{\mathbf{u}}, \dot{\phi}] = \int_V [W'(\dot{\epsilon}_{ij}) + \kappa(\dot{\phi}\dot{\mathbf{u}}_{k,k} - \frac{1}{2}\dot{\phi}^2)] dV - \int_{S_T} \dot{T}_i \dot{u}_i dS_T, \quad (4.1)$$

where

$\dot{\epsilon}_{ij} \equiv \frac{1}{2}(\dot{u}_{i,j} + \dot{u}_{j,i}) - \frac{1}{3}\delta_{ij}\dot{u}_{k,k}$ is the deviatoric strain increment,
 $W'(\dot{\epsilon}_{ij})$ is the deviatoric rate potential [$W' = \frac{1}{2}\dot{s}_{ij}\dot{\epsilon}_{ij}$; $\delta W' = \dot{s}_{ij}\delta\dot{\epsilon}_{ij}$],
 $\dot{\phi}$ is the (independent) dilatational strain increment,
 κ is the (instantaneous) bulk modulus.

This functional is well defined if a finite bulk modulus κ exists.

That this functional corresponds to a valid variational principle is readily proved in the usual way. By taking the first variations in \dot{u}_i and $\dot{\phi}$ one finds

$$\delta I = \int_V (\dot{s}_{ij}\delta\dot{\epsilon}_{ij} + \kappa\dot{\phi}\delta\dot{u}_{k,k}) dV - \int_{S_T} \dot{T}_i\delta\dot{u}_i dS_T + \int_V \kappa(\dot{u}_{k,k} - \dot{\phi})\delta\dot{\phi} dV, \quad (4.2)$$

and since

$$\dot{\sigma}_{ij} = \dot{s}_{ij} + \kappa\dot{\phi}\delta_{ij}, \quad (4.3)$$

this can be written

$$\delta I = \int_V \dot{\sigma}_{ij}\delta\dot{u}_{i,j} dV - \int_{S_T} \dot{T}_i\delta\dot{u}_i dS_T + \int_V \kappa(\dot{u}_{k,k} - \dot{\phi})\delta\dot{\phi} dV. \quad (4.4)$$

The first two terms express the virtual work principle and hence imply that $\dot{\sigma}_{ij}$ satisfy the continuing equilibrium equations in V and force rate boundary conditions on S_T in the usual manner. The last term provides the additional result that $\dot{\phi} = \dot{u}_{k,k}$.

It is appropriate to compare the present principle with the principle created by Herrmann [5] for the analysis of incompressible, linear elastic materials. The functional used by Herrmann would have the incremental form

$$H = H[\dot{u}, \dot{h}] = \int_V \mu[\dot{\epsilon}_{ij}\dot{\epsilon}_{ij} + 2\nu\dot{h}\dot{\epsilon}_{kk} - \nu(1-2\nu)\dot{h}^2] dV - \int_{S_T} \dot{T}_i\dot{u}_i dS_T, \quad (4.5)$$

where μ is the shear modulus, ν is Poisson's ratio, and where the "mean pressure function" is given by

$$\dot{h} = \frac{\dot{\sigma}_{kk}}{2\mu(1+\nu)}. \quad (4.6)$$

Apart from its specialization to linear elasticity, the fact that $\dot{\epsilon}_{kk}$ enters Herrmann's principle quadratically is an essential difference. Indeed, this does not allow for it the same simple procedures that can be based on the present principle and that allow the easy adaption of existing conventional stiffness programs to it.

Before going to the application of the principle, let us determine how many constraints per element would be *desired*, in order to get an as close as possible approximation to continuum behavior. In the continuum, each material point represents two (in problems of plane strain or axisymmetric problems) or three (in three-dimensional problems) degrees of freedom. For incompressibility, one constraint is valid at each material point. Hence the ratio of degrees of freedom to constraints in the continuum is equal to two or three, depending on the type of problem.

It seems plausible that a finite element solution to an elastic-plastic problem would give the best overall approximation if the ratio degrees of freedom to constraints would be the same as in the continuum. Hence a "two" would be desired in the last column of table 1 and a "three" in the last column of table 2. This readily leads to a *desired* number of constraints per element. For instance, for the 4-noded quadrilateral elements in table 1, the desired number would be one, and for the 8-noded quadrilateral elements, it would be three. Similarly, for the 8-noded cube in table 2, one constraint would be desired. Similar desired numbers can be obtained for the other elements in the tables.

Now let us for the moment restrict the discussion to those elements for which the desired number of constraints is equal to one. As has been discussed before, one then needs a dilatation increment governed by a single parameter. It is, on the other hand, necessary for convergence that at least a constant dilatational strain increment be obtainable within an element (see, for instance, [7]). Hence, it is necessary to choose in an element α

$$\dot{\phi} = \dot{\phi}_\alpha = \text{constant} . \quad (4.7)$$

Substitution of (4.7) in (4.1) then furnishes

$$I = \sum_{\alpha=1}^P \int_{V_\alpha} [W'(\dot{e}_{ij}) + \kappa \dot{\phi}_\alpha \dot{u}_{k,k} - \frac{1}{2} \kappa \dot{\phi}_\alpha^2] dV_\alpha - \int_{S_T} \dot{T}_i \dot{u}_i dS_T . \quad (4.8)$$

Variation of $\dot{\phi}_\alpha$ then yields the relation

$$\dot{\phi}_\alpha = \int_{V_\alpha} \kappa \dot{u}_{k,k} dV_\alpha / \int_{V_\alpha} \kappa dV_\alpha . \quad (4.9)$$

In practically all cases the bulk modulus κ will be constant within an element; in problems of non-dilatational plasticity, for instance, $\kappa = \kappa_{el}$ is a constant, and may be brought outside the integral in (4.9) so that

$$\dot{\phi}_\alpha = V_\alpha^{-1} \int_{V_\alpha} \dot{u}_{k,k} dV_\alpha . \quad (4.10)$$

Substitution of (4.10) in (4.8) then furnishes the modified functional

$$\bar{I} = \sum_{\alpha=1}^P \int_{V_\alpha} \left[W'(\dot{e}_{ij}) + \frac{1}{2} \kappa \left(V_\alpha^{-1} \int_{V_\alpha} \dot{u}_{k,k} dV_\alpha \right)^2 \right] dV_\alpha - \int_{S_T} \dot{T}_i \dot{u}_i dS_T . \quad (4.11)$$

This functional can be simplified by defining the modified strain increment

$$\begin{aligned} \dot{\bar{e}}_{ij} &= \dot{e}_{ij} + \dot{\phi} \delta_{ij} \\ &= \frac{1}{2} (\dot{u}_{i,j} + \dot{u}_{j,i}) + \frac{1}{3} \delta_{ij} \left(V_\alpha^{-1} \int_{V_\alpha} \dot{u}_{k,k} dV_\alpha - \dot{u}_{k,k} \right) \end{aligned} \quad (4.12)$$

so that the functional (4.11) can be written as

$$\bar{I} = \sum_{\alpha=1}^p \int_{V_{\alpha}} W(\dot{\bar{\epsilon}}_{ij}) dV_{\alpha} - \int_{S_T} \dot{T}_i \dot{u}_i dS_T, \quad (4.13)$$

where W represents the total rate potential (i.e. $\delta W(\dot{\epsilon}) = \dot{\sigma}_{ij} \delta \dot{\epsilon}_{ij}$), but evaluated for the modified strain increment $\dot{\bar{\epsilon}}_{ij}$. It should be observed that the functional (4.13) may be expressed purely in terms of nodal displacement increments; hence no additional variables (i.e. mean pressure) have to be used. It should also be noted that the functional is identical to the usual rate potential functional with the exception of the relation between strain and displacement increments. As was mentioned before, this makes it extremely simple to adapt an already existing program for this method. One need only rewrite the matrix converting nodal parameters to strains in accord with (4.12). An equally simple formulation cannot be obtained with Herrmann's variational principle.

It is interesting to note that the frequently employed procedure of replacing the radially-varying strains in axisymmetric triangular elements by their values at the element centroid could be viewed as being based on a variational principle similar to the present one, in both cases implemented by changing the strain-displacement relationship.

For element types for which the desired number of constraints is larger than one, the situation is only slightly more complicated. Consider for instance the 8-noded quadrilateral plane strain element. For this element type, the desired number of constraints is equal to three. A possible choice for $\dot{\phi}_{\alpha}$ is then

$$\dot{\phi}_{\alpha} = \dot{\phi}_{\alpha}^0 + (x - x_0) \dot{\phi}_{\alpha}^x + (y - y_0) \dot{\phi}_{\alpha}^y, \quad (4.14)$$

where $\dot{\phi}_{\alpha}^0$, $\dot{\phi}_{\alpha}^x$ and $\dot{\phi}_{\alpha}^y$ are constants, and x_0 , y_0 is the centroid of the element. Following a procedure similar to the one followed before, one readily derives the relations

$$\begin{aligned} \dot{\phi}_{\alpha}^0 &= V_{\alpha}^{-1} \int_{V_{\alpha}} \dot{u}_{k,k} dV_{\alpha}, \\ \dot{\phi}_{\alpha}^x &= I_{x_{\alpha}}^{-1} \int_{V_{\alpha}} (x - x_0) \dot{u}_{k,k} dV_{\alpha}, \\ \dot{\phi}_{\alpha}^y &= I_{y_{\alpha}}^{-1} \int_{V_{\alpha}} (y - y_0) \dot{u}_{k,k} dV_{\alpha}, \end{aligned} \quad (4.15)$$

where $I_{x_{\alpha}}$ and $I_{y_{\alpha}}$ are the moments of inertia around the x_0 and y_0 axes. A similar procedure can be followed for the 8-noded quadrilateral axisymmetric element and the 20-noded cube. In each case $\dot{\bar{\epsilon}}_{ij}$ is defined analogously to (4.12) in terms of nodal displacements, and the incremental stiffness equations are derived in the usual way from (4.13).

Finally it should be noted that only the quadrilateral or cubic elements have a desired number of constraints which corresponds to a simple and symmetric choice of the dilatational strain increments. For the triangular or tetrahedral elements the desired number of constraints does not

make such a simple choice possible. If we did not already know that the six-noded plane strain triangle was suitable for incompressible analysis, we would conclude, for example, that the desired number of constraints is two, which does not correspond to a complete symmetric development of the dilatational strain increments.

Because the most significant errors in computed overall load-deflection curves occur in the fully plastic range, where the deformation gradients may no longer be infinitesimal, a rigorous finite strain finite element formulation may in some cases be required. An implementation of the variational principle presented here for such a formulation is given in Appendix 2. It may also be noted that the present variational principle, eq. (4.1), may be put in a mean stress form by letting $\kappa\phi = \bar{q}$, say, be the variable, and this is suitable for strictly incompressible materials ($\kappa \rightarrow \infty$).

5. Numerical examples

In order to examine the results of the analyses of the preceding sections in specific numerical solutions, plane strain beam bending, the thick-walled plane strain tube under internal pressure, and the tensile analogue of the Prandtl punch problem were solved.

For the first type of problem, the kinematic requirement of pure bending that plane sections remain plane was enforced, so it was necessary to examine only one row of elements across the beam thickness. Ten square 4-noded isoparametric elements were placed across the thickness. Displacement boundary conditions were imposed, and the total moment was computed from the calculated nodal tractions. The material was modeled as elastic-perfectly plastic with a Poisson's ratio of 0.3. The problem was also solved by applying identical boundary conditions to a mesh of the constant dilatation isoparametrics developed in Section 4, and to a mesh composed of 10 squares, each of which was composed of 4 diagonally crossed triangles, as presented in Section 3.

The results are shown in fig. 8. The limit moment for plane strain, assuming a Mises yield condition, is simply

$$M_{limit} = \frac{2}{\sqrt{3}} \sigma_0 \left(\frac{h}{2} \right)^2, \quad (5.1)$$

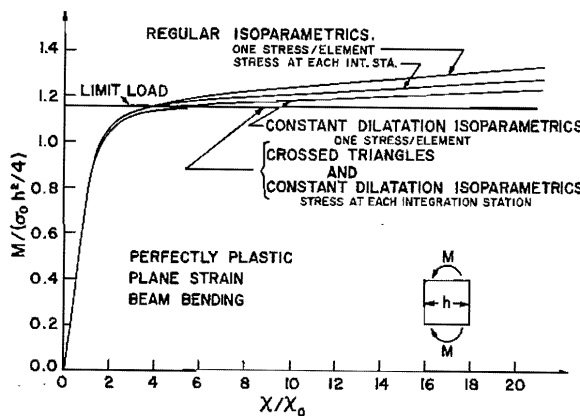


Fig. 8. Moment-curvature curves obtained from finite element solutions of perfectly plastic plane strain beam bending.

where σ_0 is the tensile yield stress and h is the beam thickness. The beam curvature χ is normalized with respect to χ_0 , the curvature necessary to bring the outer beam fibers to yield.

As can be seen, the ordinary isoparametric element does not find a limit load at all; all elements across the thickness reach yield, and the moment-curvature curve continues to rise. The steepest curve shown in fig. 8 is the case for which one stress state per element, calculated at the element centroid, is used to represent the stress state throughout the element. The next steepest curve results from calculating and storing the stresses at two thickness-direction Gaussian integration stations per element.

The third steepest curve is the result of using the constant dilatation quadrilateral element with one stress state per element. Finally, the two essentially coincident curves which actually find the correct limit load are the results of the crossed triangles and the constant dilatation quadrilaterals, calculating and storing the stress state within each element at each Gaussian integration station.

We may interpret these results by recalling that point-wise incompressibility is a *necessary* but not *sufficient* condition for a limit load to exist in the finite element model. In fact, it is also necessary that, at limit load, all deviatoric strain increments be normal (pointwise) to the yield surface. However, it is not in general possible for the constant dilatation quadrilateral to deform in a manner so that the deviatoric strain increment, which is permitted to vary within the element, be pointwise normal to a single stress state on the yield surface. When the stress state was calculated and stored at the Gaussian integration stations, however, the computed deviatoric stress increments tended to vanish in the fully plastic range for both the regular and constant dilatation isoparametrics. In fact, the difference between the terminal slopes of the moment-curvature relations for one versus four stress measures per element was identical for the regular and constant dilatation isoparametrics.

Thus, for this particular problem, the relative magnitudes of the errors in the terminal load-deflection curve associated with failure to meet the necessary conditions of pointwise incompressibility and pointwise normality of deviatoric strain increments in isoparametric quadrilaterals are given, respectively, by the terminal slopes of the second and third steepest curves of fig. 8.

The same problem was also solved for the case of linearly hardening material behavior, with a hardening modulus of one-hundredth the elastic modulus. In this problem, a constant terminal slope to the moment-curvature relation is readily calculable. The results are shown in fig. 9, where it is seen that the ordinary isoparametric element formulation exhibits much too stiff a response in the fully plastic range, a result discussed previously. The essentially coincident terminal slopes of the moment-curvature curves exhibited by both the constant dilatation quadrilaterals and the crossed triangles were less than one percent in error from the analytical terminal slope.

The beam-bending problems were also solved with ten irregularly-shaped constant dilatation quadrilaterals across the thickness, and the results were essentially unaffected.

The thick-walled plane strain tube under internal pressure proved a less dramatic example of the analysis of the preceding sections. A 10-degree sector of a tube with outer diameter to inner diameter ratio of two was modeled with five quadrilateral elements, the nodes having equal radial spacing. The problem was also solved with the same quadrilaterals formed from four triangles with the additional node lying at the intersection of the diagonals of the quadrilateral. Radial displacement increments were prescribed at the two nodes on the inner diameter, and all boundary nodal displacements were constrained to be radial in direction. Pressures were inferred in the virtual work sense from the nodal forces at the two inner-diameter nodes.

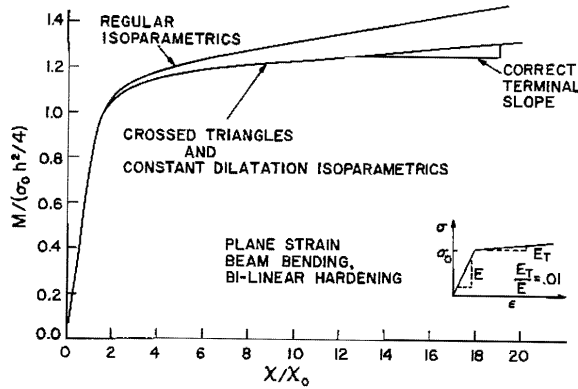


Fig. 9. Moment-curvature curves obtained from finite element solutions of linearly hardening plane strain beam bending.

The trend in load-displacement curves obtained was the same as in the beam-bending problem. However, the quantitative differences between loads at a given deformation were greatly reduced. In fact, the maximum difference in any computed load at any point in the deformation was less than four percent. The load obtained when "steady state" conditions were reached was within a few percent of the known limit load, and the pressure-expansion curves agreed closely with that obtained by Hodge and White [9] using finite differences and presented graphically in [10].

Finally, the problem of the plane strain deep, double-edge-notched (DEN) tensile specimen, shown in fig. 10, was solved using a very fine mesh of first regular then constant dilatation isoparametrics. This problem is the tensile analogue of Prandtl's punch problem (see, for example, [10]). In this case, the limit load in terms of the net stress on the ligament is given by

$$\sigma_{lim} = (2 + \pi) \sigma_0 / \sqrt{3} \approx 2.97 \sigma_0 \quad (5.2)$$

for the von Mises yield criterion, where σ_0 is again the uniaxial tension yield strength.

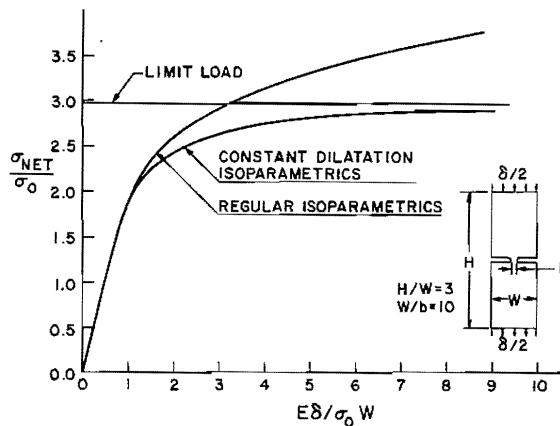


Fig. 10. Load-displacement curves obtained from finite element solutions of a deep double edge notched tensile specimen.

By symmetry, only one-fourth of the DEN specimen was analyzed. The specimen width to ligament width ratio was $W/b = 10$. The loading was accomplished by imposing increments of constant end displacement at the upper end of the specimen. The load was computed both from the nodal tractions along the top row of nodes and from the average stresses in the top row of elements. Both methods gave essentially the same results.

Fig. 10 shows the load-displacement curves as computed from the two finite element formulations. As can be seen, the ordinary isoparametric elements fail to find the correct limit load, and, in fact, the load-deflection curve continues to rise at roughly constant rate, exceeding the limit value by approximately 25% at the point for which computation was stopped. Indeed, this large error has accumulated at an end displacement of only about 5 times the displacement given by extrapolating the linear elastic loading line to the limit load.

The load-deflection curve obtained from the mesh of constant dilatation quadrilateral elements is indistinguishable from that of the regular isoparametric elements up to roughly 60% of the limit load, at which point it begins to decrease in slope more rapidly. As the deformation proceeds into the fully plastic region the difference between the two load-deflection curves increases rapidly. At the point at which computation was stopped, the load was approximately 3% less than the analytical limit load, and the tangent modulus load-deflection slope was roughly 0.1% of its elastic value, versus an apparently not decreasing 5% for the regular isoparametric elements.

Acknowledgement

The authors are grateful for financial support of this work by the U.S. National Aeronautics and Space Administration, under Grant NGL 40-002-080 to Brown University.

Appendix I: Incompressibility effects in finite element meshes

The condition $\dot{\epsilon}_{kk} = 0$, pointwise, has been shown in the text to enforce the unrealistic constraint on rectangular plane strain 4-node isoparametric elements that $\dot{\epsilon}_{xx}$ and $\dot{\epsilon}_{yy}$ must be the same for every element of the grid, and, if the 4-node isoparametrics are arbitrarily skewed quadrilaterals, then the shear strain increment rate $\dot{\epsilon}_{xy}$ must also be the same in every element.

In this appendix, the consequences of $\dot{\epsilon}_{kk} = 0$ pointwise will be examined for some other typical mesh configurations in both two and three dimensions to demonstrate the unrealistic constraints which are enforced upon admissible displacement rate fields.

Consider the array of triangular constant strain elements shown in fig. 11, and generated by single skewing of a rectangular grid. Since $\dot{\epsilon}_{xx} + \dot{\epsilon}_{yy} = 0$, one can go from element to element along the band of elements marked * and show that $\dot{\epsilon}_{xx}$ and $\dot{\epsilon}_{yy}$ are the same in every element of such a band.

Consider a rectangular array of 8-noded, three dimensional isoparametric elements, shown in fig. 12. The displacement rate field within such an element can be expressed as

$$\begin{pmatrix} \dot{u}_x \\ \dot{u}_y \\ \dot{u}_z \end{pmatrix} = \mathbf{a} + \mathbf{b}x + \mathbf{c}y + \mathbf{d}z + \mathbf{e}xy + \mathbf{f}yz + \mathbf{g}zx + \mathbf{h}xyz. \quad (\text{A1.1})$$

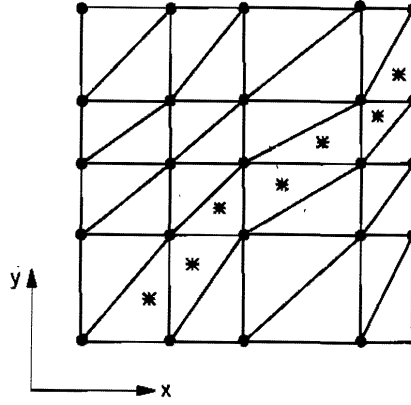


Fig. 11. Propagation of incompressibility constraints in a rectangular mesh of singly skewed constant strain triangular finite elements.

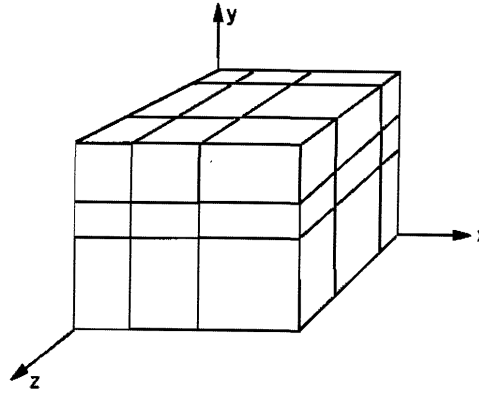


Fig. 12. Three-dimensional block of rectangular eight-node isoparametric brick finite elements.

The incompressibility constraint, namely

$$\dot{\epsilon}_{xx} + \dot{\epsilon}_{yy} + \dot{\epsilon}_{zz} = \frac{\partial \dot{u}_x}{\partial x} + \frac{\partial \dot{u}_y}{\partial y} + \frac{\partial \dot{u}_z}{\partial z} = 0, \quad (\text{A1.2})$$

requires that $\mathbf{b} = 0$ and that the other terms be constrained such that the direct strains vary linearly within the element according to

$$\begin{aligned} \dot{\epsilon}_{xx} &= p - \beta y + \gamma z \\ \dot{\epsilon}_{yy} &= q - \alpha x - \gamma z \\ \dot{\epsilon}_{zz} &= -(p + q) + \alpha x + \beta y, \end{aligned} \quad (\text{A1.3})$$

where p, q, α, β , and γ are constants within an element and are expressible in terms of nodal coordinates and displacement increment rates of a kind compatible with the incompressibility constraint.

Now consider any inter-element interface of the kind $z = \text{constant}$. The tangential strains $\dot{\epsilon}_{xx}$ and $\dot{\epsilon}_{yy}$ must be continuous across the interface and, because $\dot{\epsilon}_{zz} = -(\dot{\epsilon}_{xx} + \dot{\epsilon}_{yy})$ always, so must $\dot{\epsilon}_{zz}$ be continuous across the interface. But from (A1.3), since $\dot{\epsilon}_{zz}$ does not vary with z within an element, and since $\dot{\epsilon}_{zz}$ is continuous across element boundaries, we therefore have the constraint that $\dot{\epsilon}_{zz}$ has the same value at all points along a line extending in the z -direction. That is, $\dot{\epsilon}_{zz}$ is independent of z , and by similar reasoning $\dot{\epsilon}_{xx}$ is independent of x , and $\dot{\epsilon}_{yy}$ is independent of y .

In fact, by further considerations of continuity, it may be shown that the normal strain rates throughout the entire array are given by equations of the kind

$$\begin{aligned}\dot{\epsilon}_{xx} &= B(y) - C(z), \\ \dot{\epsilon}_{yy} &= C(z) - A(x), \\ \dot{\epsilon}_{zz} &= A(x) - B(y),\end{aligned}\tag{A1.4}$$

where $A(x)$, $B(y)$, and $C(z)$ are each continuous functions of their respective arguments, varying linearly within elements.

To see how severely this constrains admissible incremental deformation fields, suppose that the plane $z = 0$ corresponds to a fixed boundary on which all displacements must be zero. Then $\dot{\epsilon}_{xx}$ and $\dot{\epsilon}_{yy}$ vanish on this plane and, by the argument advanced earlier, so does $\dot{\epsilon}_{zz}$. Hence, from (A1.4),

$$\begin{aligned}A(x) - B(y) &= 0, \\ C(0) - A(x) &= 0, \\ B(y) - C(0) &= 0,\end{aligned}\tag{A1.5}$$

which requires that $A(x) = B(y) = C(0)$, and hence the most general admissible deformation field for the entire array of elements is

$$\begin{aligned}\dot{\epsilon}_{yy} &= -\dot{\epsilon}_{xx} = C(z) - C(0), \\ \dot{\epsilon}_{zz} &= 0.\end{aligned}\tag{A1.6}$$

If we further suppose that the plane $x = 0$ also coincides with a fixed boundary, then

$$\dot{\epsilon}_{xx} = \dot{\epsilon}_{yy} = \dot{\epsilon}_{zz} = 0\tag{A1.7}$$

throughout.

Appendix 2: Generalization to finite deformations

For the class of elastic-plastic materials deformed at finite strain which admit the existence of a constitutive rate potential, Hill [11] has shown that the solution of boundary value problems can be obtained from the following variational principle, and an Eulerian finite-element formulation for problems of large plastic flow has recently been based upon it [12, 13]:

$$\delta \left[\int_V U(D_{ij}) dV - \frac{1}{2} \int_V \left[\sigma_{ij} 2D_{ik} D_{kj} - \frac{\partial v_k}{\partial x_i} \frac{\partial v_k}{\partial x_j} \right] dV - \int_{S_T} \dot{T}_i v_i dS_T \right] = 0. \quad (A2.1)$$

Here V is the current (deformed) volume, and S_T is the portion of the current boundary on which nominal traction rates \dot{T}_i based on the current state as the reference state are prescribed. The rate of deformation tensor is D_{ij} , σ_{ij} is the Cauchy (true) stress tensor, and $\partial v_i / \partial x_j$ is the velocity gradient with respect to current coordinates. The function $U(D_{ij})$ is homogeneous of degree 2 in D_{ij} and has the property that

$$\dot{\tau}_{ij} = \frac{\partial U}{\partial D_{ij}} = \mathcal{L}_{ijkl} D_{kl}. \quad (A2.2)$$

Here \mathcal{L}_{ijkl} are the instantaneous moduli appropriate to the adopted measure of stress rate, and are possibly dependent on the direction of D_{ij} . The stress rate itself, $\dot{\tau}_{ij}$, is the Jaumann, or co-rotational, rate of Kirchhoff stress, based on a reference state that has been chosen to coincide instantaneously with the current state, and Kirchhoff stress τ_{ij} is defined as σ_{ij} times the ratio of reference state to current material density, so that $\tau_{ij} = \sigma_{ij}$ instantaneously. Note that the existence of U requires that moduli have the symmetry

$$\mathcal{L}_{ijkl} = \mathcal{L}_{klij}, \quad (A2.3)$$

and this ensures a symmetric incremental stiffness matrix for the corresponding finite element equations. The class of materials which admit rate potentials include all elastic materials for which a strain energy function exists, and also all elastic-plastic materials which satisfy the normality rule when phrased in terms of work conjugate stress and finite strain measures [14].

A generalization of the Prandtl–Reuss equations for finite deformation [12, 13] which admits the rate potential U is obtained by relating the Jaumann rate of Kirchhoff stress to the rate of deformation tensor in the usual Prandtl–Reuss form:

$$D_{ij}^e = \frac{1+\nu}{E} \dot{\tau}_{ij} - \frac{\nu}{E} \delta_{ij} \dot{\tau}_{kk}, \quad (A2.4)$$

$$D_{ij}^p = \frac{9\tau'_{ij}\tau'_{kl}\dot{\tau}_{kl}}{4h\bar{\tau}^2},$$

and

$$D_{ij} = D_{ij}^e + D_{ij}^p$$

for continued plastic loading. Here $\bar{\tau}^2 = \frac{3}{2} \tau'_{ij} \tau'_{ij}$ and h is the slope of the stress-logarithmic plastic strain curve for simple tension. Note that in this case and for other plastically incompressible materials $\bar{\tau}'_{ij}$ differs from $\bar{\sigma}'_{ij}$ only by the term $(1 - 2\nu) \sigma_{ij} \dot{\sigma}_{kk} / E$, and this is negligible by comparison for almost all technological applications of the theory to metals.

Thus equations (A2.4) can be inverted, and the resulting Jaumann rates of Kirchhoff stress separated into hydrostatic and deviatoric parts to give

$$\bar{\tau}'_{ij} = \frac{E}{1 + \nu} \left[D'_{ij} - \alpha \frac{3\tau'_{ij} \tau'_{kl} D'_{kl} \left(\frac{E}{1 + \nu} \right)}{2\bar{\tau}^2 \left(\frac{2h}{3} + \frac{E}{1 + \nu} \right)} \right], \quad \bar{\tau}'_{kk} = \frac{E}{1 - 2\nu} D_{kk} = 3\kappa D_{kk}, \quad (\text{A2.5})$$

where $\alpha = \begin{cases} 1 & \text{if at yield and } \tau'_{kl} D'_{kl} > 0 \\ 0 & \text{otherwise} \end{cases}$.

Thus the deviatoric and hydrostatic Jaumann rates of Kirchhoff stress have functional dependence only on the deviatoric and hydrostatic parts of the rate of deformation tensor, respectively.

From these relations, the volume integral of the rate potential $U = \frac{1}{2} \bar{\tau}'_{ij} D_{ij}$ in (A2.1) can be separated into deviatoric and hydrostatic parts to obtain

$$\int_V \frac{1}{2} \bar{\tau}'_{ij} D_{ij} dV = \int_V \left[\frac{1}{2} \bar{\tau}'_{ij} D'_{ij} + \frac{1}{2} \kappa D_{kk}^2 \right] dV. \quad (\text{A2.6})$$

Because this integrand has the same functional form as the conventional small-strain rate potential for Prandtl–Reuss materials, the variational principle of Section 4 can be readily generalized by replacing the term $\frac{1}{2} \kappa D_{kk}^2$ in (A2.6) with $\kappa (D_{kk} \dot{\phi} - \frac{1}{2} \dot{\phi}^2)$, as in (4.1). As in the text, independent variation of the velocities and of $\dot{\phi}$ furnishes $\dot{\phi} = D_{kk}$, the dilatation rate.

The finite element implementation of the finite strain version of the variational principle of Section 4 then follows straightforwardly, with the total element stiffness matrix being the sum of the stiffness corresponding to the modified rate potential and the “initial stress” stiffness, which corresponds to the second volume integral of (A2.1).

References

- [1] J.H. Argyris, Continua and discontinua, Proc. 1st Conf. Matrix Methods Struct. Mech. (Wright-Patterson Air Force Base, Ohio, October, 1965);
P.V. Marcal and I.P. King, Elastic-plastic analysis of two-dimensional stress systems by the finite element method, Intern. J. Mech. Sci. 9 (1967) 143–155;
O.C. Zienkiewicz, S. Vallipian and I.P. King, Elasto-plastic solutions of engineering problems, Initial-stress, finite element approach, Intern. J. Num. Meth. in Eng. 1 (1969) 75–100.
- [2] J.H. Argyris and D.W. Scharpf, Methods of elastoplastic analysis, ZAMP 23 (1972) 517–552.
- [3] K. Iwata, K. Osakada and S. Fujino, Analysis of hydrostatic extrusion by the finite element method, Trans. ASME, Ser. B, J. of Eng. for Ind. 94 (1972) 697–703.
- [4] D.M. Tracey, On the fracture mechanics analysis of elastic-plastic materials using the finite element method, Ph.D. Thesis, Brown University, Providence, R.I., (1973).

- [5] L.R. Herrmann, Elasticity equations for incompressible and nearly incompressible materials by a variational theorem, *AIAA J.* 3 (1965) 1896–1900.
- [6] O.C. Zienkiewicz, *The finite element method in engineering science* (McGraw-Hill, London, 1971).
- [7] C.S. Desai and J.F. Abel, *Introduction to the finite element method* (Van Nostrand Reinhold, New York, 1972).
- [8] E. Reissner, On a variational theorem in elasticity, *J. Math. Phys.* 24 (1950) 90–95.
- [9] P.G. Hodge, Jr. and G.N. White, Jr., A quantitative comparison of flow and deformation theories of plasticity, *J. Appl. Mech.* 17 (1950) 180–184.
- [10] W. Prager and P.G. Hodge, Jr., *Theory of perfectly plastic solids* (Dover, New York, 1968).
- [11] R. Hill, Some basic principles in the mechanics of solids without a natural time, *J. Mech. Phys. Solids* 7 (1959) 209–225.
- [12] R.M. McMeeking and J.R. Rice, Finite element formulations for problems of large elastic-plastic deformation, in preparation.
- [13] R.M. McMeeking, An Eulerian finite element formulation for problems of large displacement gradients, Sc.M. Thesis, Brown University, Providence, R.I., (1974).
- [14] R. Hill, On constitutive inequalities for simple materials, I and II, *J. Mech. Phys. Solids* 16 (1968) 229–242, 315–332.

Note Added in Proof: Dr. S.W. Key has informed us of his development of a variational principle for elastic materials which presents an alternative to Herrmann's principle in the same form as our eq. (4.1). He does not comment on the way this may be implemented within standard programs by simple redefinition of the strain-nodal displacement relations, as discussed in connection with our eqs. (4.11–4.13), but this may be done also with his approach. Key's work is published in: *Int. J. Solids Structures* 5 (1969) 951–964.